

# Clump morphology and evolution in MHD simulations of molecular cloud formation

R. Banerjee<sup>1</sup>, E. Vázquez-Semadeni<sup>2</sup>, P. Hennebelle<sup>3</sup> and R.S. Klessen<sup>1</sup>

<sup>1</sup>Zentrum für Astronomie der Universität Heidelberg, Institut für Theoretische Astrophysik, Albert-Ueberle-Str. 2, 69120 Heidelberg, Germany

<sup>2</sup>Centro de Radioastronomía y Astrofísica (CRyA), Universidad Nacional Autónoma de México, Morelia, Michoacán, Mexico

<sup>3</sup>Laboratoire de radioastronomie millimétrique (UMR 8112 CNRS), École Normale Supérieure et Observatoire de Paris, 24 rue Lhomond, 75231 Paris Cedex 05, France

25 October 2018

## ABSTRACT

We study the properties of clumps formed in three-dimensional weakly magnetized magneto-hydrodynamic simulations of converging flows in the thermally bistable, warm neutral medium (WNM). We find that: (1) Similarly to the situation in the classical two-phase medium, cold, dense clumps form through dynamically-triggered thermal instability in the compressed layer between the convergent flows, and are often characterised by a sharp density jump at their boundaries though not always. (2) However, the clumps are bounded by *phase-transition fronts* rather than by contact discontinuities, and thus they grow in size and mass mainly by accretion of WNM material through their boundaries. (3) The clump boundaries generally consist of thin layers of thermally unstable gas, but these layers are often widened by the turbulence, and penetrate deep into the clumps. (4) The clumps are approximately in both ram and thermal pressure balance with their surroundings, a condition which causes their internal Mach numbers to be comparable to the bulk Mach number of the colliding WNM flows. (5) The clumps typically have mean temperatures  $20 \lesssim \langle T \rangle \lesssim 50$  K, corresponding to the wide range of densities they contain ( $20 \lesssim n \lesssim 5000 \text{ cm}^{-3}$ ) under a nearly-isothermal equation of state. (6) The turbulent ram pressure fluctuations of the WNM induce density fluctuations that then serve as seeds for local gravitational collapse within the clumps. (7) The velocity and magnetic fields tend to be aligned with each other within the clumps, although both are significantly fluctuating, suggesting that the velocity tends to stretch and align the magnetic field with it. (8) The typical mean field strength in the clumps is a few times larger than that in the WNM. (9) The magnetic field strength in the densest regions within the clumps ( $n \sim 10^4 \text{ cm}^{-3}$ ) has a mean value of  $B \sim 6 \mu\text{G}$  but with a large scatter of nearly two orders of magnitude, implying that both sub- and super-critical cores are formed in the simulation. (10) In the final stages of the evolution the clumps' growth drives them into gravitational instability, at which point star formation sets in, and the pressure in the clumps' centers increases even further.

**Key words:** magneto-hydrodynamics, ISM: clouds, evolution, methods: numerical

## 1 INTRODUCTION

The formation of molecular clouds by converging flows in the warm neutral atomic medium (WNA) has been intensively studied in recent years through numerical and analytical treatments (e.g., Ballesteros-Paredes et al. 1999; Hennebelle & Pérault 1999; Koyama & Inutsuka 2000; Hartmann et al. 2001; Koyama & Inutsuka 2002; Audit & Hennebelle 2005; Heitsch et al. 2005; Gazol et al. 2005; Vázquez-Semadeni et al. 2006, 2007; Hennebelle et al. 2007; Heitsch et al. 2008), which have shown that molecular regions can form by ther-

mal instability TI (Field 1965) in the warm neutral interstellar medium (ISM), nonlinearly triggered by transonic compressions in the WNA. The added ram pressure of such compressions causes the affected regions to overshoot from cold neutral medium (CNM) to molecular cloud physical conditions. However, the nature and evolution of the clumps appearing self-consistently within the clouds produced by this mechanism remains controversial. On the one hand, the clumps have been reported to be in approximate pressure balance with their surroundings and to have sharp bound-

aries, as in the classical two-phase medium (e.g., Audit & Hennebelle 2005; Hennebelle et al. 2007), while simultaneously, the whole medium exhibits turbulent behavior, with wide distributions of the density and pressure. This implies the existence of significant amounts of gas in the unstable density and temperature ranges, which has been suggested to be in transit between the stable warm and cold phases (Vázquez-Semadeni et al. 2000; Gazol et al. 2001; Sánchez-Salcedo et al. 2002; Vázquez-Semadeni et al. 2003; de Avillez & Breitschwerdt 2004; Gazol et al. 2005; Audit & Hennebelle 2005).

This coexistence of a two-phase and a turbulent regime, to which we refer as “thermally bistable turbulence”, is intriguing, since turbulence implies continuous and irregular transport of gas (e.g., Klessen et al. 2000; Klessen & Lin 2003), while the two-phase regime is usually thought to imply static conditions of the clouds, held under confinement by the pressure of the warmer, more diffuse WNM, and with the two phases being mediated by contact discontinuities at pressure equilibrium, which, by definition, imply no fluid transport across them.

In this contribution, we address these issues by means of three-dimensional (3D), adaptive mesh refinement (AMR), *magneto*-hydrodynamical (MHD), self-gravitating simulations, performed with the FLASH code (Fryxell et al. 2000), which allow us to have sufficient resolution to simulate the formation of a large dense cloud complex while still resolving the interiors of the clumps that naturally form during this process. Note that, even though our simulations are magnetic, in this paper we focus on the nature and evolution of the clumps, rather than on the effect of the presence of the magnetic field, a task that we defer to a future study.

## 2 NUMERICAL MODEL

We model the convergence of WNM flows as two colliding, large-scale cylindrical streams, whose evolution we follow with the FLASH code under ideal MHD conditions. Our setup is similar (though not identical) to the non-magnetic SPH simulation of Vázquez-Semadeni et al. (2007) labeled L256 $\Delta v$ 0.17 (see their Fig. 1). Each stream is 112 pc long and has a radius of 32 pc. They are embedded in a (256 pc)<sup>3</sup> simulation box. Although the numerical box is periodic, the cloud occupies a relatively small volume far from the boundaries, and so the cloud can interact freely with its diffuse environment, with relatively little effect from the boundaries.

The cylindrical streams are given an initial, slightly supersonic inflow velocity so that they collide at the centre of the numerical box. The inflow speed of each stream corresponds to an isothermal Mach number of 1.22, where the initial temperature of the atomic gas is 5000 K implying an isothermal<sup>1</sup> sound speed of 5.7 km s<sup>-1</sup>. We also add 10% random velocity perturbations to the bulk stream speeds. The initially homogeneous density is  $n = 1 \text{ cm}^{-3}$  ( $\rho = 2.12 \times 10^{-24} \text{ g cm}^{-3}$ , using a mean atomic weight of 1.27).

<sup>1</sup> Note that our inflow speeds are a factor of  $(5/3)^{-1/2}$  smaller than the one in Vázquez-Semadeni et al. (2007) as we use the isothermal sound speed, while those authors used the adiabatic one.

Here, we report on the results from our weakly magnetised case with a homogeneous magnetic field component of strength  $B_x = 1 \mu\text{G}$ , which is parallel to the gas streams. These initial conditions translate to a plasma  $\beta = P_{\text{therm}}/P_{\text{mag}}$  of 17.34. We choose this relatively weak field so that the gas in the streams is magnetically supercritical, and thus the cloud formed by compression along the field lines can eventually also become supercritical. Note that the only way in which our clouds can become supercritical is by accreting mass from the inflows along the field lines (Mestel 1985; Hennebelle & Pérault 2000; Hartmann et al. 2001; Shu et al. 2007; Vázquez-Semadeni 2007), since we do not include ambipolar diffusion in our simulations. In any case our choice of the initial uniform field is not overly low, as recent estimates of the mean Galactic field give upper and lower limits of  $4 \pm 1$  and  $1.4 \pm 0.2 \mu\text{G}$ , respectively (Beck 2001). On the other hand, total magnetic field strengths which also comprise of field fluctuations are typically reported to be of the order of  $6 \mu\text{G}$  (see e.g., Heiles & Troland 2005). Here, we are not including initial field fluctuations. In our simulation, such fluctuations are dynamically generated in the CNM from the initial turbulent velocity and thermal instability.

This setup is different from the numerical setup in our companion paper, Hennebelle et al. (2008), where a significantly stronger field was used ( $5 \mu\text{G}$ ), and the colliding streams entered the simulation box along the field direction through two opposite boundaries, which had inflow rather than periodic conditions. Thus, in that paper, the mass-to-flux ratio of the cloud was allowed to increase without limit, while in our simulations, this ratio is bounded from above by the mass-to-flux ratio of the simulation box.

These initial conditions result in a ratio of the total mass in the flows,  $M_{\text{flows}} \approx 2.26 \times 10^4 M_{\odot}$ , to the thermal Jeans mass of  $M_{\text{flows}}/M_J \approx 2 \times 10^{-3}$ . The warm neutral medium is far from being gravitationally unstable. On the other hand, the mass-to-flux ratio of the flows,  $\mu = M_{\text{flows}}/\Phi_B = \Sigma/B_x$ , is such that  $\mu/\mu_{\text{crit}} \approx 2.9$ , where  $\mu_{\text{crit}} \approx 0.13/\sqrt{G}$  is the critical value for a slightly flattened structure on the verge of collapse (Mouschovias & Spitzer 1976; Spitzer 1978). Using this critical value, the mass-to-flux ratio of the *entire* simulation box is  $3.3 \mu_{\text{crit}}$ , because the extend of the flows is slightly smaller than the box size. We estimate the transition time at which the cloud becomes magnetically super-critical as

$$t_{\text{trans}} \approx 5.4 \text{ Myr} \times \left( \frac{n}{1 \text{ cm}^{-3}} \right)^{-1} \left( \frac{v_{\text{flow}}}{6.9 \text{ km s}^{-1}} \right)^{-1} \left( \frac{B_x}{1 \mu\text{G}} \right). \quad (1)$$

Concerning the cooling, we use the procedure described in Vázquez-Semadeni et al. (2007), which is based on the chemistry and cooling calculations of Koyama & Inutsuka (2000) and the analytic fits to them by Koyama & Inutsuka (2002). Thermal conduction is neglected.

We follow the gravitational collapse with up to 11 AMR refinement levels, which correspond to a maximum resolution of 8192 grid points<sup>2</sup>, or a grid spacing of  $\Delta x = 0.03 \text{ pc}$  in each direction. For the dynamical mesh refinement we use a Jeans’ criterion, where we resolve the local Jeans’ length

<sup>2</sup> Note, each refinement level corresponds to a block  $8^3$  grid points

with at least 10 grid cells (see Truelove et al. 1997, for the necessary criterion to prevent artificial fragmentation). It should be noted that some authors have advocated that the resolution criterion should be to resolve the Field length (Field 1965) with at least three grid points (Koyama & Inutsuka 2004; Gressel 2009). Other authors (Hennebelle & Audit 2007) have suggested that the proper scale that needs to be resolved is the “sound crossing scale”, the product of the sound speed and the cooling time. In the warm and cold atomic phases, either of these criteria may actually be more stringent than the Jeans one but, as also discussed by Hennebelle & Audit (2007), the main effect of insufficient resolution in this kind of simulations is to truncate the fragmentation at the smallest resolved scales, in turn causing the the low-mass end of the clump mass spectrum to be also truncated. However, in this paper we are not concerned with resolving small scale fluctuations nor in the detailed shape and extension of the core spectrum, but rather with the mechanism of clump growth, and the clumps’ substructure, once they have reached well-resolved sizes. As discussed by Vázquez-Semadeni et al. (2006), the physics of clump growth are simple, and do not require a very high resolution. In that paper, it was also concluded that, since clumps grow, they are necessarily unresolved during the initial stages of their formation, but later become well resolved, as they reach sufficiently large sizes. Thus, we can investigate the substructure of clumps that have had enough time to become well resolved. Nevertheless, it could be that by also resolving small scale fluctuations the conversion of the WNM to the CNM might be slightly faster if the surface-to-volume ratio of the cold gas increases in this case. On the other hand, since we plan to use the present simulations to study the star formation process in future contributions, it is important to satisfy the Jeans criterion. In any case, our clumps are typically resolved with at least the 10th level of refinement, corresponding to a resolution of 0.06 pc.

Finally, Lagrangian sink particles (see e.g., Bate et al. 1995; Jappsen et al. 2005) are created if the local density exceeds  $n > n_{\text{sink}} \equiv 2 \times 10^4 \text{ cm}^{-3}$  and this location is a local minimum of the gravitational potential. These particles interact only gravitationally with the gas and with each other. They are free to move within the simulation box independent of the underlying mesh (i.e Lagrangian particles). The sink particles have an accretion radius of 0.47 pc corresponding to roughly one Jeans’ length at  $n_{\text{sink}}$ . Within this accretion radius, gas in excess of  $n_{\text{sink}}$  is deposited into the sink if this gas is gravitationally bound. The sink mass increases accordingly. Note that the initial mass of the sink is computed with the dynamically accreted mass; i.e., only the mass in excess of  $n_{\text{sink}}$  contributes to the initial sink mass.

In a forthcoming study we investigate the influence of ambipolar diffusion (AD) on molecular cloud formation in colliding flows, where we are using the implementation of ambipolar diffusion for the FLASH code by Duffin & Pudritz (2008). Ambipolar diffusion might regulate the magnetic field strength in the condensations that are induced by thermal instability (Inoue et al. 2007; Inoue & Inutsuka 2008).

## 3 RESULTS

### 3.1 Global features

As is already well known, the collision of transonic, converging flows initially produces moderate compressions on the *linearly stable* WNM at the collision front, which are sufficiently strong to nonlinearly trigger thermal instability (Hennebelle & Pérault 1999), so that the gas rapidly cools to temperatures well below 100 K, forming a thin sheet that then fragments into filaments and ultimately into small clumps. Moreover, the thermal pressure of the dense gas is in close balance with the thermal + ram pressure of the WNM outside it, and it is at higher densities and pressures than the steady-state CNM, overshooting to typical giant molecular cloud physical (density and temperature) conditions (Vázquez-Semadeni et al. 2006,  $n \sim 100 \text{ cm}^{-3}$ ,  $T \sim$  a few tens of Kelvins). This process also causes the newly formed dense gas to be turbulent, with a transonic velocity dispersion with respect to its own sound speed (Koyama & Inutsuka 2002; Heitsch et al. 2005; Vázquez-Semadeni et al. 2006; Hennebelle et al. 2008). As in the classical two-phase model (Field et al. 1969), the clumps in the dense gas are bounded by sharp density jumps of roughly a factor of 100. We refer to this regime of global turbulence subjected to the tendency to form dense clumps by TI as “thermally bistable turbulence”. In what follows, we indistinctly refer to the dense clumps as “molecular”, even though we do not actually follow the chemistry in our simulations.

In this regime, the “molecular cloud” is composed of a mixture of diffuse and dense gas, with a significant fraction of gas in the unstable range, which is in transit from the diffuse to the dense phase, thus producing a continuous though bimodal distribution of densities and temperatures (Vázquez-Semadeni et al. 2000; Gazol et al. 2001, 2005; Audit & Hennebelle 2005). In Fig. 1 we show the structure of the dense cloud from our converging flow simulation about 5 Myr after the first regions collapse and form stars. In particular, from the face-on image one can see that the “cloud” is not a homogeneous entity, but rather it is composed of dense clumps (which should be mostly molecular) embedded in somewhat less dense filaments (which may be partly molecular and partly atomic) (see also Vázquez-Semadeni et al. 2007; Hennebelle et al. 2008).

### 3.2 Clump properties

#### 3.2.1 Clump growth mechanism

As mentioned above, the clumps are mainly bounded by sharp density jumps of roughly a factor of 100. However, the clumps are connected to large filaments which build up in the intersection region of the colliding flows. The main difference between the regime in the simulations and the classical two-phase model of Field et al. (1969) is that, because the clumps are formed by turbulent compressions in the WNM rather than by linear development of TI, *they can accrete mass from distances much larger than the scale of the fastest-growing mode of TI in the diffuse medium*, which is typically small. In a turbulent environment, instead, the clumps can accrete from the scales associated with the compressive motion that forms the clumps. This implies that, for turbulence-induced clump formation, the duration of clump

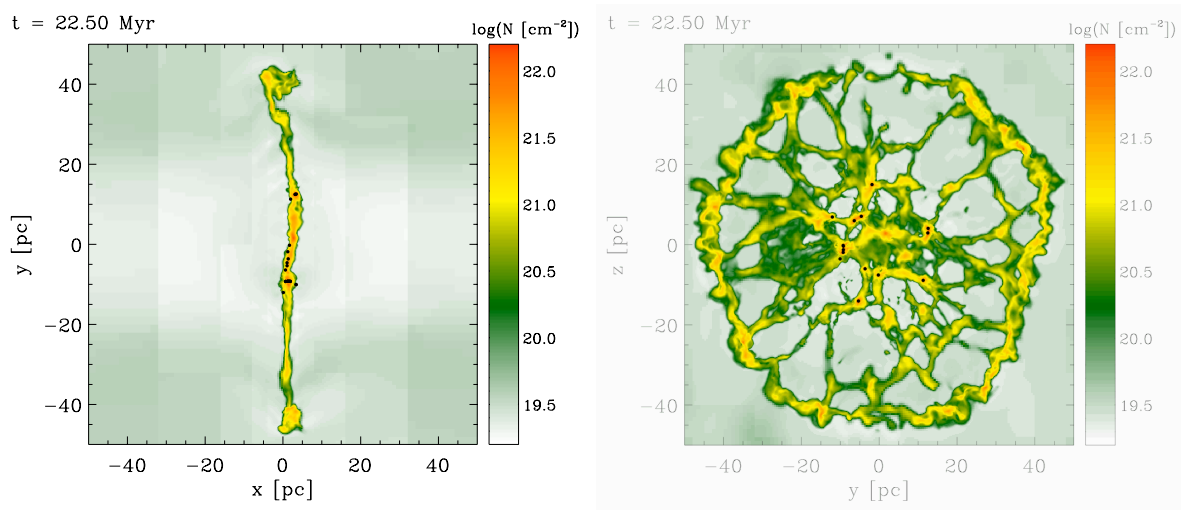


**Figure 1.** Column density of the inner region of the molecular cloud viewed edge-on (left panel) and face-on (right panel). In the left panel, the large scale flows advance inwards from the right and left sides of the box, leaving a lower-density medium there. In both panels, the dots mark the projected positions of the sink particles, i.e. regions of local gravitational collapse. The first regions that show active star formation appear at about 17 Myr in this simulation. The molecular cloud is largely inhomogeneous, with the “molecular” gas ( $\log(N/\text{cm}^{-2}) \gtrsim 20.5$ ) interspersed within the warm atomic gas. Note that the simulation box is 4 times larger (i.e. 256 pc each side) than the area shown here.

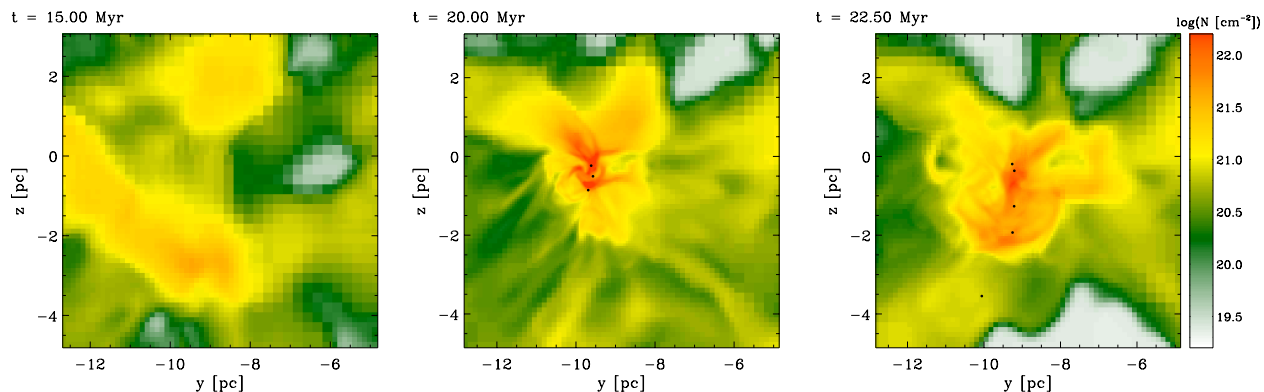


**Figure 2.** Column density evolution of a clump (colored yellow-green) in which a self gravitating, cold, dense core (yellow-red) builds up. The clump is embedded in a large-scale, filamentary structure (see also Fig. 1) but is separated from the external WNM (light-blue) by a sharp boundary (dark green), although it exhibits a complex, fluctuating substructure. The clump grows mainly by accretion of material from the WNM. Cold, dense regions become Jeans unstable and start to form stars (indicated by the black dots). See also Fig. 6.

growth may be much longer than in the case of linear development, and thus one should expect to generally find the clumps in a growing stage, rather than in a quasi-static state, as in the final state of the linear development of TI. In turn, this means that there should generally be a net mass flux across their boundaries driven by the *ram* pressure of the inflow. This dynamic growth is different to the situation in the quasi-static two-phase model, in which any mass flux through the fronts (evaporation or condensation; e.g., Zeldovich & Pikel’Ner 1969) occurs as a result of the tendency to equalize the *thermal* pressure between the CNM and the WNM. We thus refer to the clumps’ boundaries as *phase transition fronts*.

This mechanism has been studied in detail in one dimension by Hennebelle & Péroul (1999) and Vázquez-Semadeni et al. (2006). The latter authors gave analytical

solutions for the expansion velocity of the phase transition front that separates the warm and cold gas as a function of the bulk Mach number of the inflows (see their fig. 3). Typically, those speeds are small, because the gas is tightly packaged in the clumps, and so the clump size increases slowly. In fact, interestingly, the front speed *decreases* with increasing inflow Mach number because the ram pressure of the compression then causes the clump density to be sufficiently large as to overwhelm the larger accretion rate onto the cloud, and the net effect is that the front propagates at lower speeds. During their growth, the clumps also occasionally coalesce with other nearby clumps, a process that enhances their growth rate.

In Fig. 2 we show the column density evolution of a typical clump in our simulation, which exhibits the aforementioned sharp boundaries and growth, although large

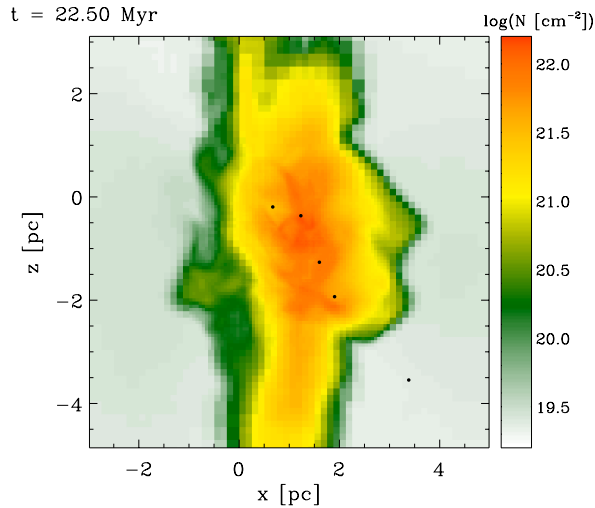


**Figure 3.** Column density of the edge-on view of the clump shown in Fig. 2. The clump clearly originates at the intersection of the large scale flows and is connected to a large filamentary structure. Perpendicular to the filament the clump grows through the propagation of its phase transition front into the WNM.



**Figure 4.** Three dimensional structure of the clump shown in the last panel of Fig. 2. The density iso-surface is shown for number density of  $600 \text{ cm}^{-3}$  reveals the complex structure of this clump.

fluctuations are seen within it as well. A few million years later, the clump becomes self-gravitating and starts to produce local sites of collapse. We also show an edge-on column density view of the clump at  $t = 22.5 \text{ Myr}$  in Fig. 3 and a 3D iso-density image in Fig. 4, which shows the complexity of the dense clump.

It is important to note that the clumps' growth mechanism is a simple consequence of the thermal bistability of the flow, triggered by the transonic compression in the WNM, so it is essentially a thermo-hydrodynamic phenomenon, independent of the presence of the magnetic field. Indeed, Fig. 5 shows the density and velocity field for a clump in a non-

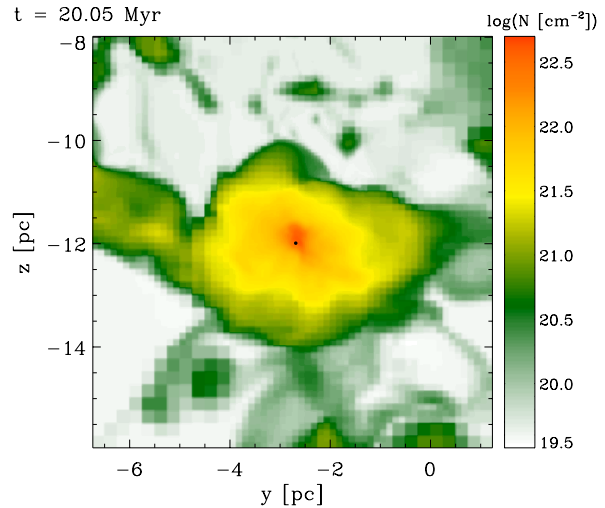


**Figure 5.** Column density of a clump from the hydro simulation. The structure of the clump and its growth by accretion of WNM material are very similar to the weakly magnetised case shown in Fig. 2.

magnetic simulation, showing that the same growth mechanism occurs there as well. The inclusion of the magnetic field does not appear to change its basic action, as the gas simply tends to flow along field lines, which in turn are re-oriented by the inertia of the flow (cf. sec. 3.2.2).

### 3.2.2 Clump internal structure

To examine the internal structure of the dense clumps, in Figs. 6 and 7 we show slices through the clump shown in the last panel of Fig. 2, at two different  $x$  positions, one through the site of its maximum density (Fig. 6), and the other closer to its periphery (Fig. 7). The four panels of each figure respectively show maps of the density, temperature, pressure, and magnetic field strength of the clump. The resolution in the interior of the clump is  $0.03 \text{ pc}$ , while its linear dimensions at  $t = 22.5 \text{ Myr}$  are seen to be roughly  $3 \times 5 \text{ pc}$ , suggesting that the clump is well resolved.

At this point, it is convenient to estimate the expected pressure-equilibrium value of the density in the clumps, when one includes the ram pressure from the colliding inflows. The density and temperature initial conditions of our simulation imply a thermal pressure  $P_{\text{th}} = 5000 \text{ K cm}^{-3}$ . From Fig. 2 of Vázquez-Semadeni et al. (2007), it can be seen that the (hydrostatic) cold-phase density corresponding to this pressure in our simulation is  $\sim 150 \text{ cm}^{-3}$ . Since the inflow speed of the colliding streams is 1.22 times the sound speed in the WNM, the ram pressure is  $\sim 1.22^2 / \sqrt{5/3} \approx 1$  times the thermal pressure,<sup>3</sup> for a total pressure of  $P_{\text{tot}} = P_{\text{th}} + P_{\text{ram}} \approx 10^4 \text{ K cm}^{-3}$ . The pressure-equilibrium density of the cold gas at this pressure is seen to be, from that figure,  $n \sim 300 \text{ cm}^{-3}$ .

<sup>3</sup> Recall the Mach number we use is with respect to the isothermal sound speed, but the calculation needs to be performed with the adiabatic one (see also Vázquez-Semadeni et al. 2006).

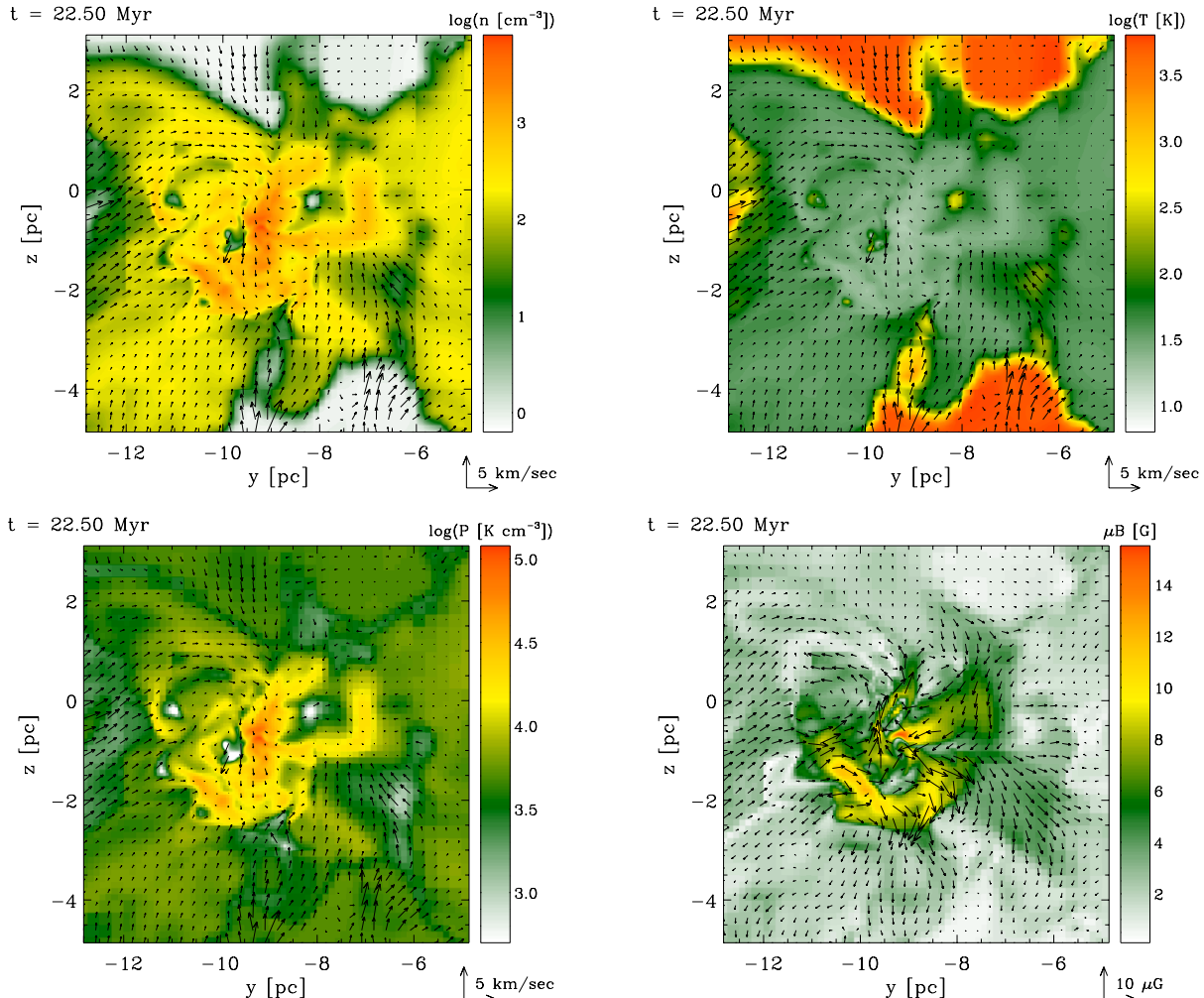


**Figure 6.** Structure of the clump shown in the right panel of Fig. 2. The images show 2D slices through the densest region of the clump. Shown are the density (top left), temperature (top right), thermal pressure (bottom left), and magnetic field strength (bottom right; note the linear scale). The arrows in the pressure image indicate the velocity field and, in the magnetic field image, the magnetic field vectors. The WNM gas streams into the clump predominately along the magnetic flux lines. Note in the top left panel that the clump boundaries (dark green) are generally thin, but on occasions become wide and penetrate deep into the core, causing the transition from WNM to CNM to “molecular” gas to be smoother.

It is then noteworthy that, although the clump is clearly separated from the WNM by a sharp boundary (dark green in the top left panels of Figs. 6 and 7), its central part (Fig. 6) contains densities ranging from  $n \sim 20 \text{ cm}^{-3}$  to  $5000 \text{ cm}^{-3}$ , and is seen to be strongly turbulent. Specifically, the few-tens-of-Kelvins gas (dark green), which is mostly associated with the clumps’ thin boundaries, is seen to often extend over much wider regions, penetrating deep into the clump structure. Presumably, this is gas in transit towards cold-phase conditions, whose transition has been delayed by the turbulence (Vázquez-Semadeni et al. 2003). Finally, note that the clump contains a few warmer, lower-density and lower-pressure “holes”, which are closer to having WNM conditions. In summary, the turbulence within the clumps, perhaps aided by self-gravity (see below), causes strong fluctuations of about one order of magnitude above and below the canonical steady-state value of the CNM density. Within this clump, the temperature is  $T \sim 20 - 50 \text{ K}$ , whereas the

surrounding warm gas is still at  $T \sim 5000 \text{ K}$ . The small variability of the temperature within the clump is consistent with the nearly-isothermal behavior of the gas at those densities. Indeed, from Fig. 2 of Vázquez-Semadeni et al. (2007), it is seen that the slope  $\gamma_e$  of the  $P$  vs.  $\rho$  curve for the dense gas is  $\sim 0.8$ , while an isothermal behavior would correspond to  $\gamma_e = 1$ .

The thermal pressure field is similarly seen to have large fluctuations within the clump, in fact exceeding those seen in the surrounding WNM. The largest values of the thermal pressure inside the clump are probably caused by the beginning of the gravitationally-contracting phase of these regions. Such large thermal pressure fluctuations are a reflection of the turbulent character of the ram pressure in the clump’s environment.

The velocity dispersion within this clump is  $\sim 0.7 \text{ km s}^{-1}$ . Estimating a sound speed of  $\sim 0.4 \text{ km s}^{-1}$  for the gas in the clump, the implied Mach number is  $\sim 1.75$ . Given

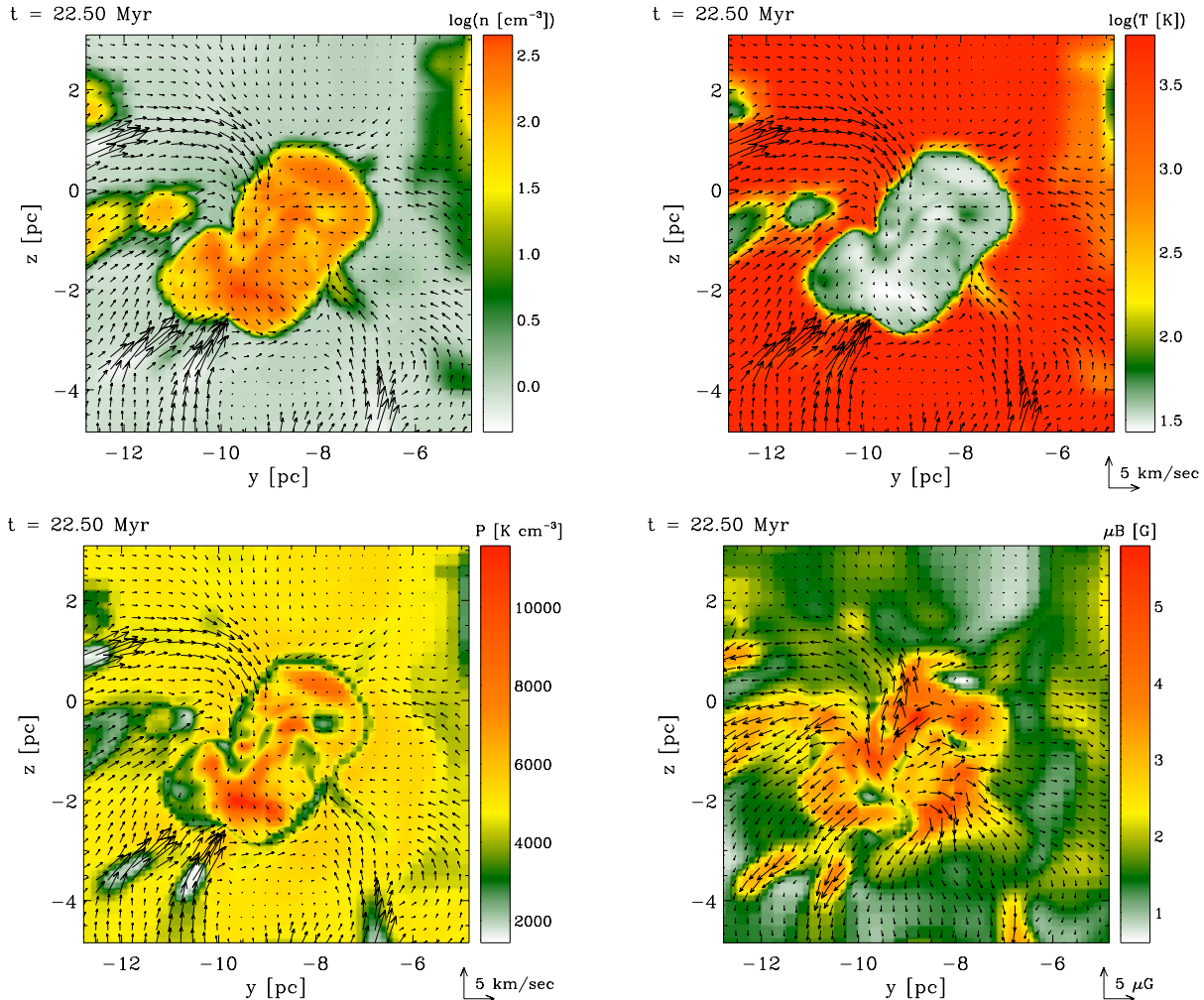


**Figure 7.** Same 2D images than shown in Fig. 6 but cut through slightly off center ( $x = 2.5$  pc, see also Fig. 3). Here the clump properties are highly distinct. In particular, the density and temperature contrast compared to the WNM is greatly prominent. Due to the thermal bistability of the flow, the clump is almost in pressure equilibrium with its surroundings.

the slightly softer-than-isothermal equation of state implies a slightly larger-than-isothermal density jump in this gas, so that, under the effect of turbulence alone, one should expect a density contrast  $\sim 5$ . The additional density enhancement may be attributed to incipient gravitational contraction. Indeed, the mass of this clump is  $\sim 280M_{\odot}$ , while the Jeans mass for density  $n = 200 \text{ cm}^{-3}$  is  $150M_{\odot}$ , indicating that the clump is undergoing gravitational contraction, also indicated by the fact that it has already formed sink particles. This is further illustrated in Fig. 8, which shows the mass  $M$  and the number of Jeans masses  $N_J$  of the gas above a given density in the region shown in the rightmost panel of Fig. 2 and in Fig. 6. It is clearly seen that the clump as a whole is gravitationally unstable, containing a couple of Jeans masses. The highest density regions do not appear Jeans unstable, but this may be a consequence of the fact that this clump has already formed sinks, so the sink mass has already been removed from the gas phase. On the other hand, the lowest-density gas within the clump ( $n \sim 20\text{--}30 \text{ cm}^{-3}$ ) is probably due to interference between the condensation process and the turbulence, causing some

accreting gas from the WNM to not be able to immediately undergo the phase transition to the cold phase.

Concerning the magnetic field, from Figs. 6 and 7, we see that it tends to be aligned with the velocity field in the dense regions, although it is also highly distorted there (recall that the initial configuration had the magnetic field parallel to the  $x$  axis), a phenomenon already observed in the 2D simulations of Passot et al. (1995). The visual impression of alignment is confirmed by the histogram of  $\mathbf{v} \cdot \mathbf{B} / |\mathbf{v}| |\mathbf{B}|$ , which is shown in Fig. 11 for all of the dense ( $n > 5 \times 10^3 \text{ cm}^{-3}$ ) gas in the simulation. The histogram clearly exhibits peaks at 1 and  $-1$ , indicating alignment. The tangling in the clumps indicates that the field has been strongly distorted by the turbulent motions in the compressed regions. In this case, the alignment with the velocity field is probably a consequence of the fact that motions non-parallel to the field tend to stretch and align it along with them (Hennebelle & Pérault 2000). A similar alignment is observed in runs with a more realistic mean field strength of  $3\mu\text{G}$ , and including an initial fluctuating component of the

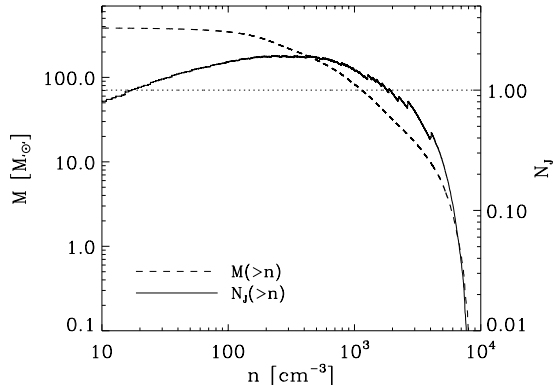


**Figure 8.** Mass  $M$  and number of Jeans masses  $N_J$  of the gas above a given density in the region shown in the rightmost panel of Fig. 2 and in Fig. 6 ( $t = 22.5$  Myr). The clump is seen to be globally gravitationally unstable (i.e., from its largest scales, which correspond to the lowest mean densities).

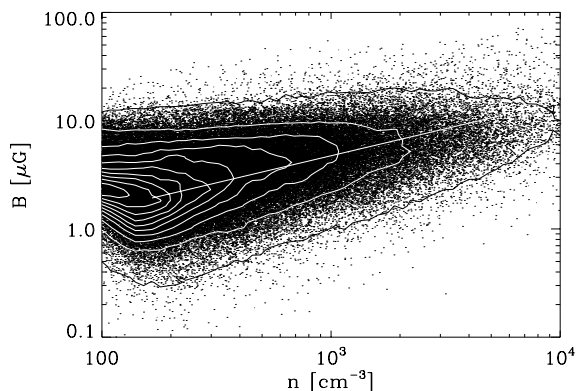
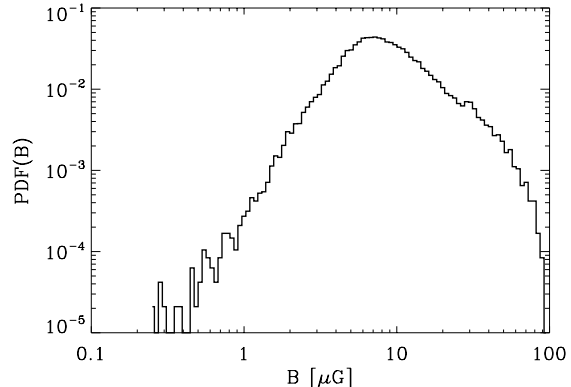


**Figure 9.** Scatter plot and two-dimensional histogram showing the magnetic field strength and density of all grid points in the simulation at  $t = 22.5$  Myr. The most probable value of the magnetic field at a given density (indicated by the locus of the rightmost apexes of the contours) is seen to scale with density roughly as  $n^{1/2}$  (straight line), although a large scatter of almost two orders of magnitude is seen around this mean trend at each density. On the other hand, the maximum magnetic field strength scales only weakly with the gas density (i.e.,  $B_{\max} \propto n^{0.15}$  for the uppermost contour line).

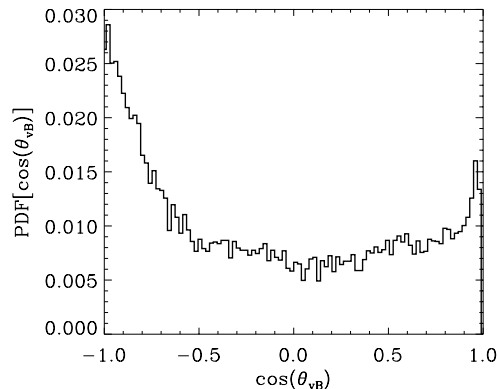
field, suggesting that this result may actually be expected to apply in actual interstellar clouds.

Fig. 9 shows a scatter plot (*dots*) and a two-dimensional histogram (*contours*) of the magnetic field strength versus the density for each pixel in the simulation. One can see that, from  $n \sim 100 \text{ cm}^{-3}$  to  $10^4 \text{ cm}^{-3}$ , the most probable value of the magnetic field, indicated by the locus of the rightmost apexes of the contours, appears to scale roughly as  $n^{1/2}$ , although with great scatter around this value.

It is worth noting that at densities  $n \sim 10^4 \text{ cm}^{-3}$ , the mean field strength is  $\langle B \rangle \sim 10 \mu\text{G}$ , although field strengths ranging from  $\sim 1$  to  $\sim 100 \mu\text{G}$  are observed. This is illustrated in Fig. 10, which shows the field strength distribution in the high density gas only ( $n \geq 5 \times 10^3 \text{ cm}^{-3}$ ). This



**Figure 10.** Probability density function of the magnetic field strength in the high density regions ( $n \geq 5 \times 10^3 \text{ cm}^{-3}$ ), showing a variability of one order of magnitude of the field strength above and below a most probable value of  $\langle B \rangle \sim 6 \mu\text{G}$  at  $t = 22.5$  Myr.



**Figure 11.** Histogram of  $\cos \theta_{vB} = \mathbf{v} \cdot \mathbf{B} / vB$  computed over all of the high-density ( $n > 5 \times 10^3 \text{ cm}^{-3}$ ) gas in the simulation, where  $v$  and  $B$  are respectively the magnitudes of the vectors  $\mathbf{v}$  and  $\mathbf{B}$  at  $t = 22.5$  Myr. The velocity and magnetic field vectors are clearly seen to show a strong tendency to be either parallel or antiparallel.

suggests that strongly as well as weakly magnetized cores should exist within the clumps, implying that some of the non-detections of the field through, for example, Zeeman measurements (Crutcher et al. 1999; Crutcher 2004), should actually correspond to very low field strengths, rather than to alignment effects that mask the field.

### 3.2.3 Statistics of mean clump properties

In order to study the collective properties of all clumps in the molecular cloud, we apply a simple algorithm to identify them in our simulation data. We define clumps as connected regions with density above a certain threshold. For comparison, we use two threshold values:  $n_{\text{thres}} = 200 \text{ cm}^{-3}$  and  $n_{\text{thres}} = 500 \text{ cm}^{-3}$ . We choose these values because they bracket the steady-state value of the density of the CNM (cf. sec. 3.2.2). We have found that the clump statistics are fairly insensitive to the different density thresholds, suggest-



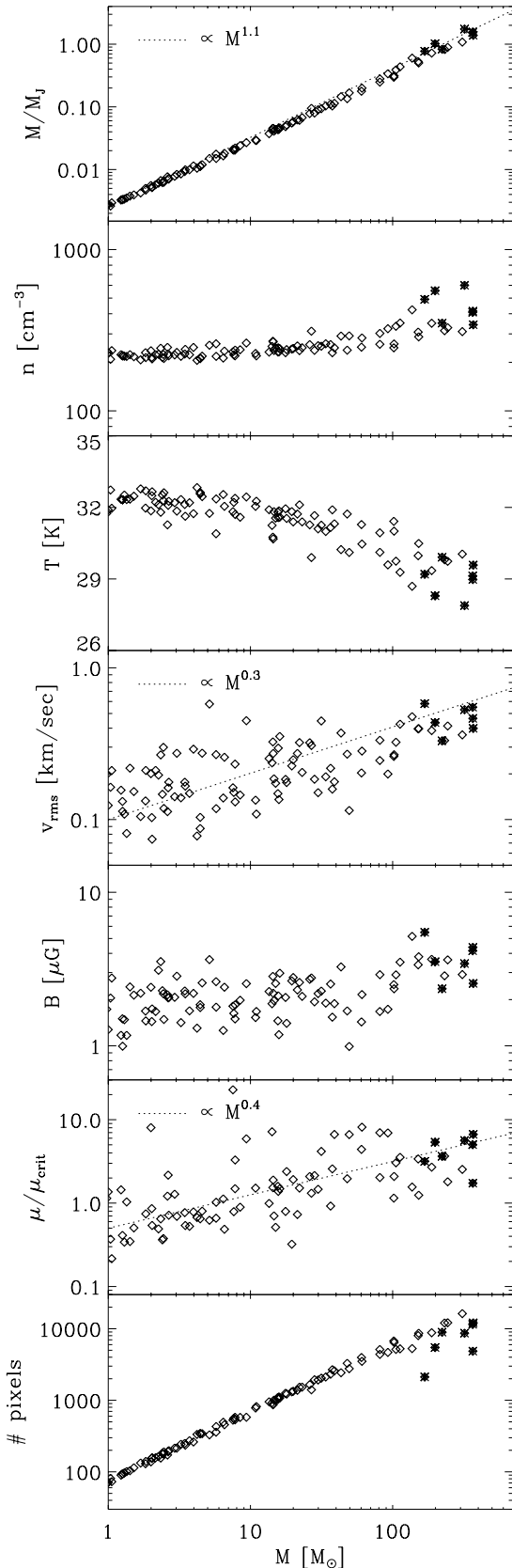


**Figure 12.** Statistical properties of the molecular clumps identified in the cloud at  $t = 22.5$  Myr. Here, we define clumps as connected regions with densities above  $200 \text{ cm}^{-3}$ . These quanti-

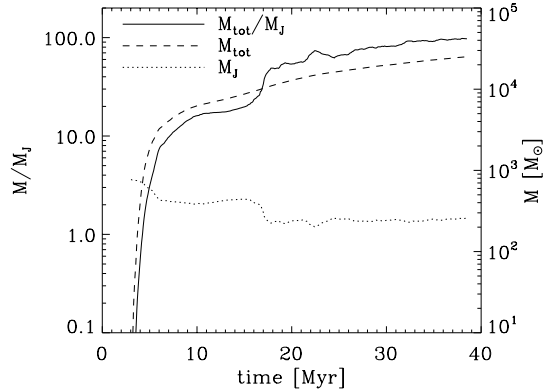


**Figure 13.** Evolution of the total cloud mass (defined as gas with density  $n > 100 \text{ cm}^{-3}$ ) and ratio of this mass to the cloud’s Jeans mass, showing that the entire cloud rapidly grows to contain a large number of Jeans masses.

ing that our results are not significantly biased by our choice of threshold.

In Fig. 12 we show some of the averaged internal properties of the clumps found in the whole cloud at  $t = 22.5$  Myr. The masses of these clumps span the range  $2 - 400 M_{\odot}$  at this time. Clumps more massive than  $\sim 200 M_{\odot}$  are close to being Jeans unstable (see the top panel of this figure, where we show the ratio  $M/M_J$  as a function of the clump mass  $M$ ). Some regions within these massive clumps are collapsing and will form stars. It is interesting, however, that the self-gravitating clumps as a whole tend to have values of  $M/M_J$  not much larger than unity. At first sight, this might appear contradictory with the notion that molecular clouds contain many Jeans masses. However, this apparent contradiction is resolved by noting that our entire cloud, formed of many clumps, does contain a large number of Jeans masses, as illustrated in Fig. 13, which shows the total mass of the cloud (defined as gas with density  $n > 100 \text{ cm}^{-3}$ ) and the ratio of this mass to its Jeans mass, clearly indicating that, by the end of the simulation, the entire cloud contains roughly 100 Jeans masses. This supports the notion that giant molecular clouds may consist of molecular clumps immersed in an atomic substrate (e.g., Goldsmith & Li 2005; Hennebelle & Inutsuka 2006).

The average density and temperature depend only weakly on the clump masses. This reflects the fact that the filling factor of the higher-density gas within the clumps is very low (i.e., most of the mass is at the lower densities), and thus the mean density of the clumps is always very close to the threshold density for defining them, with the most massive clumps having slightly larger mean densities (Vazquez-Semadeni et al. 1997). The near constancy of the clumps’ densities and temperatures is also indicated by the almost linear relation between the clumps’ masses and their ratio of mass to Jeans mass, as shown in Fig. 12.

The velocity dispersion  $\sigma$  in the clumps increases with clump mass, which, together with the fact that the clumps have roughly the same density, implies that  $\sigma$  increases with size. However, note that the dynamical range of the clump sizes is less than one decade and the scatter in the velocity data is quite large. This prevents us from fitting a proper

$\sigma$ - $L$  relation here. Estimating a typical sound speed of  $\sim 0.4 \text{ km s}^{-1}$  we find that most of the clumps are sub- or transonic. Only the most massive clumps, which are already in the state of collapse, develop larger supersonic velocities, suggesting that such velocities are the result of the gravitational collapse of the clumps, or regions within them (the cores).

The fact that the turbulence in the clumps shortly after their condensation is transonic, just as is the turbulence in the surrounding WNM, is remarkable. It appears to be consequence that the ram pressure fluctuations in the cold gas are excited by the ram pressure of the warm gas, i.e.,  $\rho_w v_w^2 \sim \rho_c v_c^2$ . In addition, the cold, dense clumps evolve quickly into thermal- pressure equilibrium with their warm surroundings (due to the thermal bistability), so that  $\rho_w c_w^2 \sim \rho_c c_c^2$ . The two conditions combined imply that the thermal Mach numbers in both media are comparable (i.e.,  $M_w \sim M_c$ ).

The typical mean field strength in the clumps exhibits an interesting dichotomy: clumps with  $M \lesssim 100 M_\odot$  have a mean field strength  $B \sim 2 \mu\text{G}$ , independent of the clump’s mass, while clumps with  $M \gtrsim 100 M_\odot$ , of which more than half have already formed sinks, have systematically larger field strengths of nearly twice that amount. This result is in agreement with observational results that the field strength is essentially independent of gas density for the WNM and CNM, and only begins to increase with density at higher densities, where presumably gravitational contraction is at work (e.g. Crutcher et al. 2003; Heiles & Troland 2005). It is nevertheless interesting that the typical field strength for the low-mass clumps is roughly twice the mean value for the whole simulation, indicating that some amount of mean field amplification exists in the clumps with respect to the WNM, even if by only a factor of  $\sim 2$ .

Finally, we note that almost all clumps with mass above  $10 M_\odot$  show a critical or super-critical mass-to-flux ratio,  $\mu$ , with a mass dependence of  $\mu \propto M^{0.25-0.4}$ ,<sup>4</sup> although this result may be an artifact of the low degree of magnetization of our simulations (recall the mean field of our magnetized simulation is  $1 \mu\text{G}$ ).

### 3.2.4 Evolution of the cloud

While the individual clumps inside the molecular cloud grow and merge, the cloud continues to accrete mass from the WNM (see Fig. 14 for the cloud mass evolution). Eventually, this leads to the global contraction of the entire cloud. In our simulation this happens at  $t \sim 20 \text{ Myr}$  which is about 15 Myr after the first dense clumps have formed. The increased gravitational potential in the centre of the cloud further compresses the gas, therefore converting an increasing amount of diffuse gas into the dense phase. This relieves concerns that the accumulation length required to attain molecular cloud-like column densities from one-dimensional accumulation of WNM gas is exceedingly long ( $\sim 1 \text{ kpc}$ ; McKee & Ostriker 2007, sec. 2.3), since much of the column

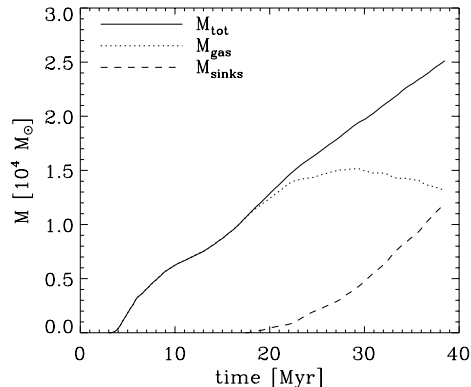


**Figure 14.** Mass evolution of the dense gas (i.e.  $n > 100 \text{ cm}^{-3}$ ,  $M_{\text{gas}}$ ), sink particles ( $M_{\text{sinks}}$ ) and their sum ( $M_{\text{tot}}$ ). The mass accretion rate of the collapsing regions increases from  $10^{-4}$  to  $10^{-3} M_\odot \text{ yr}^{-1}$  during the cloud evolution. Note that our model does not include feedback effects which should ultimately limit the star formation efficiency (e.g. see Vázquez-Semadeni et al. 2007, for an estimate of the time at which the cloud could be disrupted by the formed OB stars.)

density increase is provided by the three-dimensional gravitational compression of the gas. The importance of lateral gravitational contraction was already pointed out in Hartmann et al. (2001) and was recently also confirmed in three dimensional simulations by Heitsch & Hartmann (2008) (see also Dobbs et al. 2008). The one-dimensional compression only provides the cooling and compression necessary for self-gravity to become important, which then provides the remaining necessary compression (see also Elmegreen 2007).

The late global contraction finally leads to enhanced gas densities and large ( $\sim 10 \text{ pc}$ ), dense, coherent, and collapsing regions of mainly “molecular” gas, in which local collapse events occur before the global collapse is completed (e.g. Klessen 2001; Mac Low & Klessen 2004). Eventually, a high-density and high-velocity dispersion region forms in the overall minimum of gravitational potential, when the global collapse finally reaches center. We expect that this stage may result in the conditions where massive stars can form (e.g., Zinnecker & Yorke 2007; Vázquez-Semadeni et al. 2008, 2009).

The global evolution of our fiducial magnetic simulation, with a mean field strength of  $1 \mu\text{G}$ , is in general similar to the evolution of the non-magnetic fiducial simulation in Vázquez-Semadeni et al. (2007, run L256 $\Delta v$ 0.17 there), in the sense that the collision of the WNM flows produces a CNM cloud that, due to the combined action of compression and cooling, becomes gravitationally unstable and begins to contract and undergo collapse at localized sites. Also similar are the evolutions of the dense-gas and stellar masses (compare Fig. 14 to fig. 5 of Vázquez-Semadeni et al. 2007), and the formation of a ring at the periphery of the cloud (Burkert & Hartmann 2004). Subtle differences, however, do exist between the two simulations, due mainly to the presence of the magnetic field, albeit weak, and to the slightly weaker inflow speed of our simulation compared to that of run L256 $\Delta v$ 0.17. In particular, in the present simulation, the global collapse of the ring occurs at a signifi-

<sup>4</sup> We use the projected area of the clump,  $A_{yz}$ , and the averaged normal field component,  $\langle B_x \rangle = V^{-1} \int dV B_x$ , where  $V$  is the volume of the clump, to calculate the mass-to-flux ratio, i.e.  $\mu = M_{\text{clump}}/A_{yz} \langle B_x \rangle$ .

cantly later time than in run L256 $\Delta v$ 0.17 ( $t \sim 40$  Myr vs.  $t \sim 23$  Myr, respectively). This is possibly a consequence of the lower inflow speed, which does not cause as strong an ejection of material in the radial direction, as well as of the presence of the magnetic field, which is perpendicular to this ejection direction, both allowing a greater concentration of material in the central parts of the cloud, and a lower mass of the ring. As a consequence, in our simulation the first local collapse events occur in the central parts of the cloud, while in run L256 $\Delta v$ 0.17 they occurred in the peripheral ring.

#### 4 SUMMARY AND CONCLUSIONS

In this paper we have reported results on the physical properties of the dense gas (which we refer to as “molecular”) structures formed by transonic compressions in the diffuse atomic medium, using 3D MHD simulations including self-gravity, and radiative heating and cooling laws leading to thermal bistability of the gas. We have defined the clumps as connected regions with densities  $n \geq 200 \text{ cm}^{-3}$ , which selects the clumps formed by a phase transition from the diffuse to the dense phases of thermal instability (TI). We do not consider in our statistics the substructures within these clumps, which would correspond to dense molecular cores.

The ram pressure from the accretion of WNM gas into the clumps contributes a net ram pressure, in addition to the thermal pressure of the WNM, causing the clumps’ densities to overshoot past the typical conditions of the CNM ( $n \sim 50 \text{ cm}^{-3}$ ), well into the realm of physical conditions typical of large molecular clouds ( $n \gtrsim 200 \text{ cm}^{-3}$ ). Moreover, since the ram pressure from the diffuse medium is turbulent and fluctuating, it induces transonic turbulence within the clumps which, as a consequence of the joint conditions of ram and thermal pressure balance, must have an rms Mach number comparable to that in the diffuse gas. The transonic turbulence in the clumps induces significant density fluctuations, which then provide the seeds for subsequent local gravitational collapse as the clumps approach their Jeans mass.

We found that the transition between such clumps and the diffuse medium is generally sharp, with both media being at roughly the same thermal pressure, similarly to the situation in the classical two-phase medium of Field et al. (1969). However, the clumps contain large density fluctuations within them, of up to one order of magnitude above and below the nominal pressure-equilibrium density value, caused by the presence of thermally unstable gas still in transit towards the cold phase on the one hand, and to local gravitational contraction on the other. Thus, the boundaries of the clumps, which generally consist of thin layers of thermally unstable gas, often become extended and penetrate deep into the clumps. The clumps are nearly isothermal inside, with temperatures in the range  $\sim 20\text{--}50$  K, as consequence of the density fluctuations within the clumps and the nearly isothermal equation of state governing the high-density gas.

Another key difference between the classical model and the results of our simulations is that the clumps are formed *dynamically* by the compressions in the surrounding WNM,

implying that they are subject to continuous accretion from the WNM driven by its ram pressure (Ballesteros-Paredes et al. 1999; Ballesteros-Paredes 2006). This in turn causes the clumps’ mass and size to grow in time. Thus, the clumps’ boundaries are ram-pressure-driven *phase-transition fronts* and clump growth occurs mainly by accretion through their boundaries, rather than by coagulation, as was the case in earlier models of the ISM (e.g., Kwan & Valdes 1983). In turn, this mass flux drives the clumps to eventually become gravitationally unstable and collapse (see also Gómez et al. 2007, for an analogous situation in isothermal flows, with clumps being bounded by accretion shocks).

The magnetic field shows a significant level of alignment with the velocity field, but also large fluctuations in magnitude and direction inside the clumps, suggesting that it has been significantly distorted by the turbulent motions in the dense gas. We also find very similar distortions of the magnetic field structure by turbulent motions in the case with larger a initial field strengths of  $3 \mu\text{G}$ . This suggests that gas streams and field lines are likely to be aligned in the cases of either a weak or a strong magnetic field.

The molecular clumps and the cloud as a whole are dynamical and evolve with time, with important consequences for their ability to form stars (e.g., Mac Low & Klessen 2004; Ballesteros-Paredes et al. 2007). After some 20 Myr of evolution, some regions have already undergone local collapse and started to form stars, while other clumps do not yet show signs of star formation, similarly to the suggestion by Elmegreen (2007) for clouds behind the spiral arms of the Galaxy. From Fig. 14, we see that by  $t \sim 28$  Myr, roughly 15-20% of the total mass in the cloud (dense gas + sinks) has been converted to sinks. By this time, according to the estimates of Vázquez-Semadeni et al. (2007), based on the prescription by Franco et al. (1994), the cloud could be destroyed by the newly formed massive stars. Since SF began in the simulation at  $t \sim 17$  Myr, this implies that the stellar age spread in the *entire cloud* should be  $\sim 10$  Myr. Note, however, that our entire cloud, with a physical size of  $\sim 80$  pc is analogous to a giant cloud complex, rather than to an isolated cloud. Local, isolated SF sites of sizes  $\sim 10$  pc, have smaller age spreads.

During the evolution of the cloud, global gravitational focusing enlarges connected molecular regions in the centre of the cloud (see also Burkert & Hartmann 2004; Hartmann & Burkert 2007). At the stage when the global contraction reached the center of the cloud, we expect that the conditions should be reached where massive stars could form (see, e.g., Zinnecker & Yorke 2007; Vázquez-Semadeni et al. 2008, 2009).

We conclude that the formation and evolution of clumps in a thermally bistable medium is a highly complex process that retains some of the features from the classical two-phase model, such as the frequent presence of sharp density discontinuities, which separate the cold clumps from the warm diffuse medium, while at the same time exhibiting a much more complex structure, consisting of an intricate filament network connecting the clumps, and made up of mainly thermally unstable gas. Furthermore, the clumps are internally turbulent, and thus have density fluctuations of up to one order of magnitude even before they become gravitationally unstable. The role of the magnetic field appears negligible at the relatively low magnetization levels we have considered

in this paper. In a subsequent paper, we will consider more strongly magnetized regimes, including ambipolar diffusion.

## ACKNOWLEDGEMENTS

We thank the anonymous referee for useful comments and suggestions on our work which helped to improve this paper. The FLASH code was developed in part by the DOE-supported Alliances Center for Astrophysical Thermonuclear Flashes (ASC) at the University of Chicago. Our simulations were carried out on the Cluster Platform 4000 (Kan-Balam) at DGSCA-UNAM and at HLRB II of the Leibniz Rechenzentrum, Garching. RB is funded by the DFG under the grant BA 3607/1-1. E.V.-S. acknowledges financial support from CONACYT grant U47366-F. R.S.K. thanks for subsidies from the German Science Foundation (DFG) under Emmy Noether grant KL 1358/1 and grants KL 1358/4 and KL 1358/5. This work was supported in part by a FRON-TIER grant of Heidelberg University sponsored by the German Excellence Initiative, as well as by the Federal Ministry of Education and Research via grant 17EcCZXd.

## REFERENCES

- Audit E., Hennebelle P., 2005, *A&A*, 433, 1  
 Ballesteros-Paredes J., 2006, *MNRAS*, 372, 443  
 Ballesteros-Paredes J., Hartmann L., Vázquez-Semadeni E., 1999, *ApJ*, 527, 285  
 Ballesteros-Paredes J., Klessen R. S., Mac Low M.-M., Vázquez-Semadeni E., 2007, in Reipurth B., Jewitt D., Keil K., eds, *Protostars and Planets V Molecular Cloud Turbulence and Star Formation*. pp 63–80  
 Ballesteros-Paredes J., Vázquez-Semadeni E., Scalo J., 1999, *ApJ*, 515, 286  
 Bate M. R., Bonnell I. A., Price N. M., 1995, *MNRAS*, 277, 362  
 Beck R., 2001, *Space Science Reviews*, 99, 243  
 Burkert A., Hartmann L., 2004, *ApJ*, 616, 288  
 Crutcher R., Heiles C., Troland T., 2003, in Falgarone E., Passot T., eds, *Turbulence and Magnetic Fields in Astrophysics Vol. 614 of Lecture Notes in Physics*, Berlin Springer Verlag, *Observations of Interstellar Magnetic Fields*. pp 155–181  
 Crutcher R. M., 2004, *Ap&SS*, 292, 225  
 Crutcher R. M., Troland T. H., Lazareff B., Paubert G., Kazès I., 1999, *ApJ*, 514, L121  
 de Avillez M. A., Breitschwerdt D., 2004, *A&A*, 425, 899  
 Dobbs C. L., Glover S. C. O., Clark P. C., Klessen R. S., 2008, *MNRAS*, 389, 1097  
 Duffin D. F., Pudritz R. E., 2008, *MNRAS* in press  
 Elmegreen B. G., 2007, *ApJ*, 668, 1064  
 Field G. B., 1965, *ApJ*, 142, 531  
 Field G. B., Goldsmith D. W., Habing H. J., 1969, *ApJ*, 155, L149+  
 Franco J., Shore S. N., Tenorio-Tagle G., 1994, *ApJ*, 436, 795  
 Fryxell B., Olson K., Ricker P., Timmes F. X., Zingale M., Lamb D. Q., MacNeice P., Rosner R., Truran J. W., Tufo H., 2000, *ApJS*, 131, 273  
 Gazol A., Vázquez-Semadeni E., Kim J., 2005, *ApJ*, 630, 911  
 Gazol A., Vázquez-Semadeni E., Sánchez-Salcedo F. J., Scalo J., 2001, *ApJ*, 557, L121  
 Goldsmith P. F., Li D., 2005, *ApJ*, 622, 938  
 Gómez G. C., Vázquez-Semadeni E., Shadmehri M., Ballesteros-Paredes J., 2007, *ApJ*, 669, 1042  
 Gressel O., 2009, *ArXiv e-prints*  
 Hartmann L., Ballesteros-Paredes J., Bergin E. A., 2001, *ApJ*, 562, 852  
 Hartmann L., Burkert A., 2007, *ApJ*, 654, 988  
 Heiles C., Troland T. H., 2005, *ApJ*, 624, 773  
 Heitsch F., Burkert A., Hartmann L. W., Slyz A. D., Devriendt J. E. G., 2005, *ApJ*, 633, L113  
 Heitsch F., Hartmann L., 2008, *ApJ*, 689, 290  
 Heitsch F., Hartmann L. W., Slyz A. D., Devriendt J. E. G., Burkert A., 2008, *ApJ*, 674, 316  
 Hennebelle P., Audit E., 2007, *A&A*, 465, 431  
 Hennebelle P., Audit E., Miville-Deschênes M.-A., 2007, *A&A*, 465, 445  
 Hennebelle P., Banerjee R., Vázquez-Semadeni E., Klessen R. S., Audit E., 2008, *A&A*, 486, L43  
 Hennebelle P., Inutsuka S.-i., 2006, *ApJ*, 647, 404  
 Hennebelle P., Pérault M., 1999, *A&A*, 351, 309  
 Hennebelle P., Pérault M., 2000, *A&A*, 359, 1124  
 Inoue T., Inutsuka S.-i., 2008, *ApJ*, 687, 303  
 Inoue T., Inutsuka S.-i., Koyama H., 2007, *ApJ*, 658, L99  
 Jappsen A.-K., Klessen R. S., Larson R. B., Li Y., Mac Low M.-M., 2005, *A&A*, 435, 611  
 Klessen R. S., 2001, *ApJ*, 556, 837  
 Klessen R. S., Heitsch F., Mac Low M.-M., 2000, *ApJ*, 535, 887  
 Klessen R. S., Lin D. N., 2003, *Phys. Rev. E*, 67, 046311  
 Koyama H., Inutsuka S.-i., 2000, *ApJ*, 532, 980  
 Koyama H., Inutsuka S.-i., 2002, *ApJ*, 564, L97  
 Koyama H., Inutsuka S.-i., 2004, *ApJ*, 602, L25  
 Kwan J., Valdes F., 1983, *ApJ*, 271, 604  
 Mac Low M.-M., Klessen R. S., 2004, *Reviews of Modern Physics*, 76, 125  
 McKee C. F., Ostriker E. C., 2007, *ARA&A*, 45, 565  
 Mestel L., 1985, in Black D. C., Matthews M. S., eds, *Protostars and Planets II Magnetic fields*. pp 320–339  
 Mouschovias T. C., Spitzer Jr. L., 1976, *ApJ*, 210, 326  
 Passot T., Vázquez-Semadeni E., Pouquet A., 1995, *ApJ*, 455, 536  
 Sánchez-Salcedo F. J., Vázquez-Semadeni E., Gazol A., 2002, *ApJ*, 577, 768  
 Shu F. H., Allen R. J., Lizano S., Galli D., 2007, *ApJ*, 662, L75  
 Spitzer L., 1978, *Physical processes in the interstellar medium*. New York Wiley-Interscience, 1978. 333 p.  
 Truelove J. K., Klein R. I., McKee C. F., Holliman J. H., Howell L. H., Greenough J. A., 1997, *ApJ*, 489, L179+  
 Vázquez-Semadeni E., 2007, in Elmegreen B. G., Palous J., eds, *IAU Symposium Vol. 237 of IAU Symposium, Molecular cloud turbulence and the star formation efficiency: enlarging the scope*. pp 292–299  
 Vázquez-Semadeni E., Ballesteros-Paredes J., Klessen R. S., 2003, *ApJ*, 585, L131  
 Vázquez-Semadeni E., Ballesteros-Paredes J., Klessen R. S., Jappsen A. K., 2008, in Beuther H., Linz H., Henning T., eds, *Astronomical Society of the Pacific Confer-*

- ence Series Vol. 387 of Astronomical Society of the Pacific Conference Series, Massive Star-Forming Regions: Turbulent Support or Global Collapse?. pp 240–+
- Vázquez-Semadeni E., Ballesteros-Paredes J., Rodríguez L. F., 1997, *ApJ*, 474, 292
- Vázquez-Semadeni E., Gazol A., Passot T., et al. 2003, in Falgarone E., Passot T., eds, *Turbulence and Magnetic Fields in Astrophysics* Vol. 614 of *Lecture Notes in Physics*, Berlin Springer Verlag, *Thermal Instability and Magnetic Pressure in the Turbulent Interstellar Medium*. pp 213–251
- Vázquez-Semadeni E., Gazol A., Scalo J., 2000, *ApJ*, 540, 271
- Vázquez-Semadeni E., Gómez G. C., Jappsen A. K., Ballesteros-Paredes J., González R. F., Klessen R. S., 2007, *ApJ*, 657, 870
- Vázquez-Semadeni E., Gómez G. C., Jappsen A. K., Ballesteros-Paredes J., Klessen R. S., 2009, *arXiv:astro-ph*
- Vázquez-Semadeni E., Ryu D., Passot T., González R. F., Gazol A., 2006, *ApJ*, 643, 245
- Zeldovich Y. B., Pikel’Ner S. B., 1969, *Soviet Journal of Experimental and Theoretical Physics*, 29, 170
- Zinnecker H., Yorke H. W., 2007, *ARA&A*, 45, 481